

Supplemental Information : Understanding the nanoscale structure of hexagonal phase lyotropic liquid crystal membranes

Benjamin J. Coscia Douglas L. Gin Richard D. Noble Joe Yelk
Matthew Glaser Xunda Feng Michael R. Shirts

February 23, 2018

Further details regarding monomer parameterization

We parameterized monomers according to the following procedure:

1. *Create monomer structure file with connectivity* : We drew atomistic structures using MarvinSketch 17.13 [1] with all hydrogen atoms drawn out explicitly. We optimized the 3D geometry of the structure using the 'Clean in 3D' function of MarvinSketch. We saved the structure as a .mol file, then converted it to .pdb format using Open Babel 2.4.1 [2, 3].
2. *Assign GAFF atomtypes using antechamber* : Using the .pdb structure file as input, we ran `antechamber` [4] using the AM1-BCC charge model. The net charge on the monomer is input as -1 since the sodium ion is kept as a separate residue. We use LEaP [5] and the output of `antechamber` to create Amber topology files. A detailed tutorial can be accessed elsewhere [6].
3. *Create GROMACS topologies from Amber output* : The output of LEaP is a .inpcrd and a .prmtop file which are Amber topology files. Using acpype.py [7], we converted the LEaP output into GROMACS .gro and .top files.
4. *Perform a simulated annealing procedure on the monomer* : We created a cubic box around the monomer using the GROMACS command `gmx editconf`. The monomer was centered in the box with edges of the box spaced at least 3 nm from the monomer on all sides. We ran an energy minimization on the system with the steepest descent algorithm. Next we performed an NVT simulated annealing procedure. We linearly decreased the temperature of the system from 1000 K to 50 K over the course of 10 ns. We randomly chose a monomer configuration from the last 10 % of the trajectory.
5. *Reassign charges with molcharge* : With the monomer configuration taken from the annealed trajectory, we reassigned charges using `molcharge` with the am1bccsym method in order to ensure charges are symmetric. This condition is not guaranteed with `antechamber`. The charges in the GROMACS topology file (.top) were replaced with the new charges calculated by `molcharge`.
6. *Anneal again to get final structure* : We repeated the same simulated annealing procedure using the monomer topology with `molcharge` charges. A random monomer configuration was pulled from the last 10 % of the trajectory and was used to build all assemblies reported (Figure 1).

Calculation of pore-to-pore spacing statistics

We are interested in 5 pore-to-pore distances which should all be equal in a perfect hexagonal array (Figure 7). Only 4 of the 5 distances are independent. We can calculate a trajectory of spacing versus time for each of the 5 distances. We calculated the average pore-to-pore spacing and its uncertainty according to the following procedure:

1. We calculated the time when each of the pore-to-pore distances were equilibrated using `pymbar.timeseries.detectEquilibration()` [8, 9]. We began calculations after the largest of the five values.

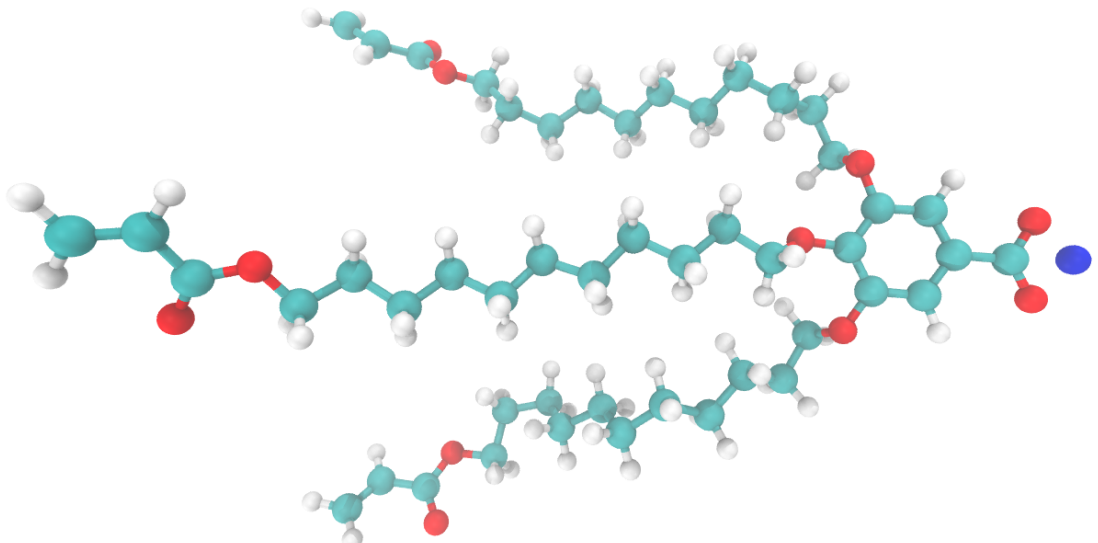


Figure 1: Atomistic representation of the monomer Na-GA3C11. White atoms represent hydrogen, cyan atoms represent carbon, red atoms represent oxygen and the blue atom is sodium.

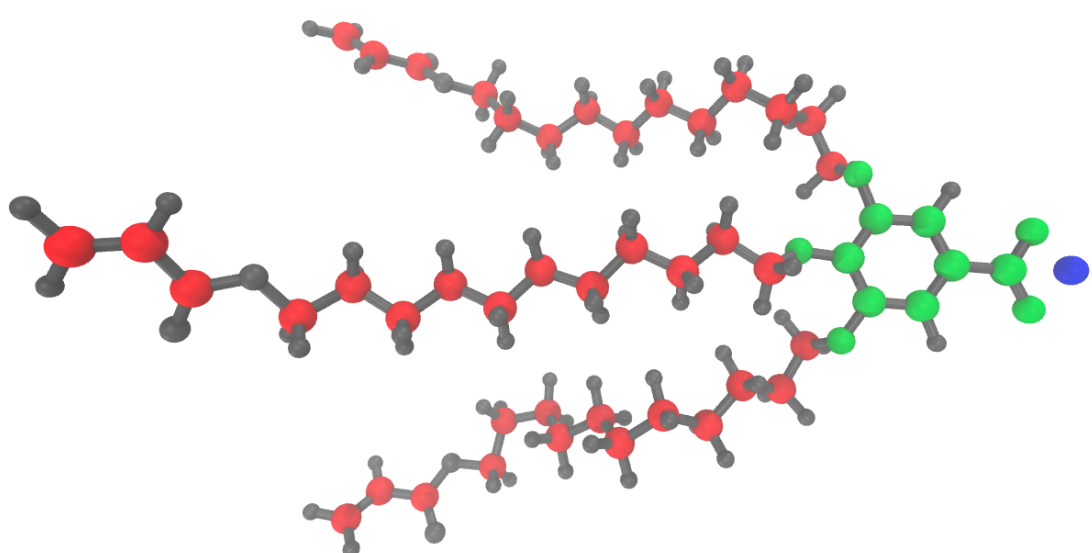


Figure 2: The groups used for $g(z)$ calculations. Red atoms are in the tails group. Green atoms are in the head group region. The blue atom is sodium.

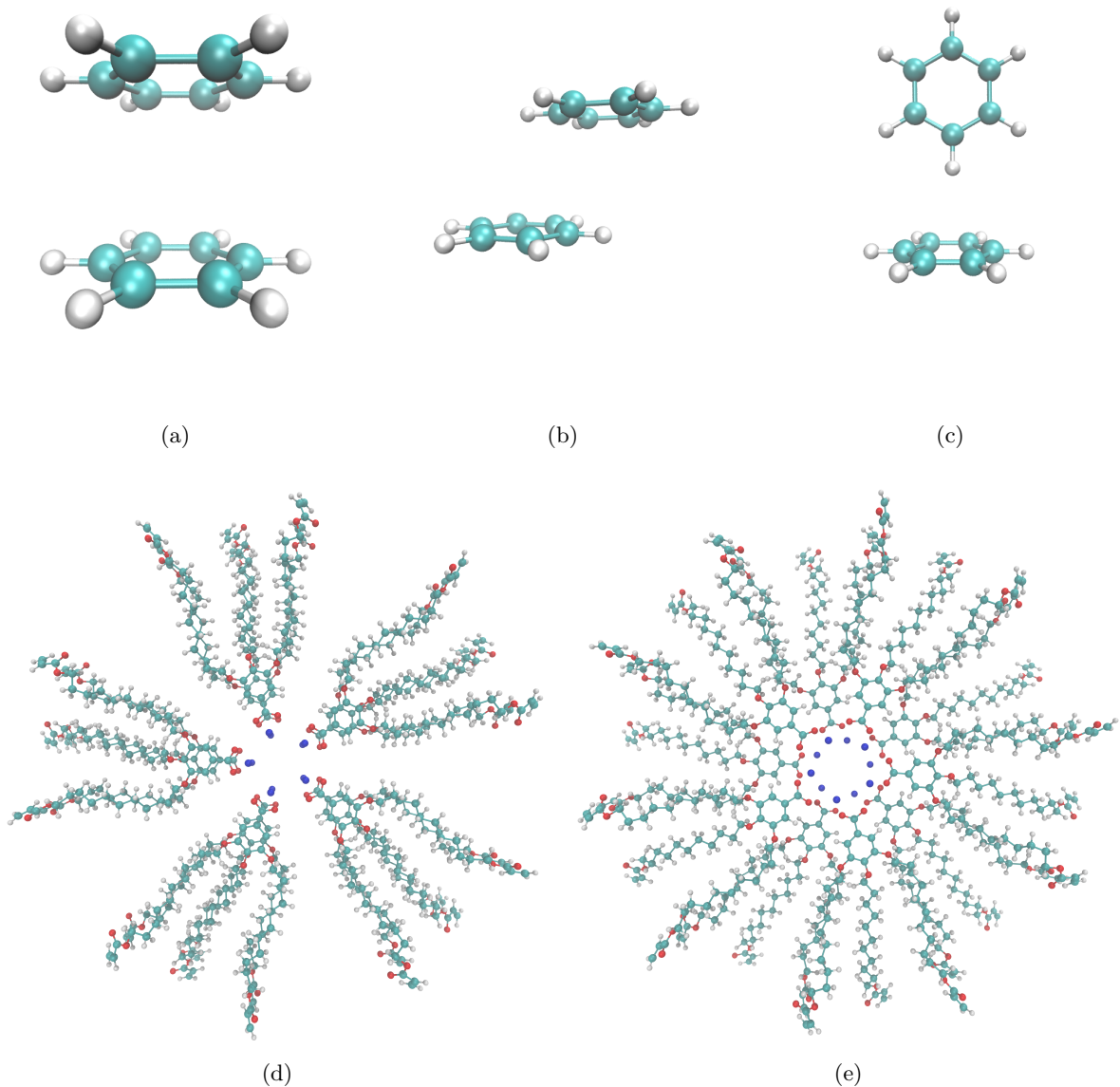


Figure 3: (a) Sandwiched benzene dimers stack 3.8 Å apart. (b) Parallel-Displaced benzene dimers stack 3.4 Å vertically and 1.6 Å horizontally apart. (c) T-shaped benzene dimers stack 5.0 Å apart. (d) Two monomer layers stacked in the sandwiched configuration (e) Two monomer layers stacked in the parallel-displaced configuration

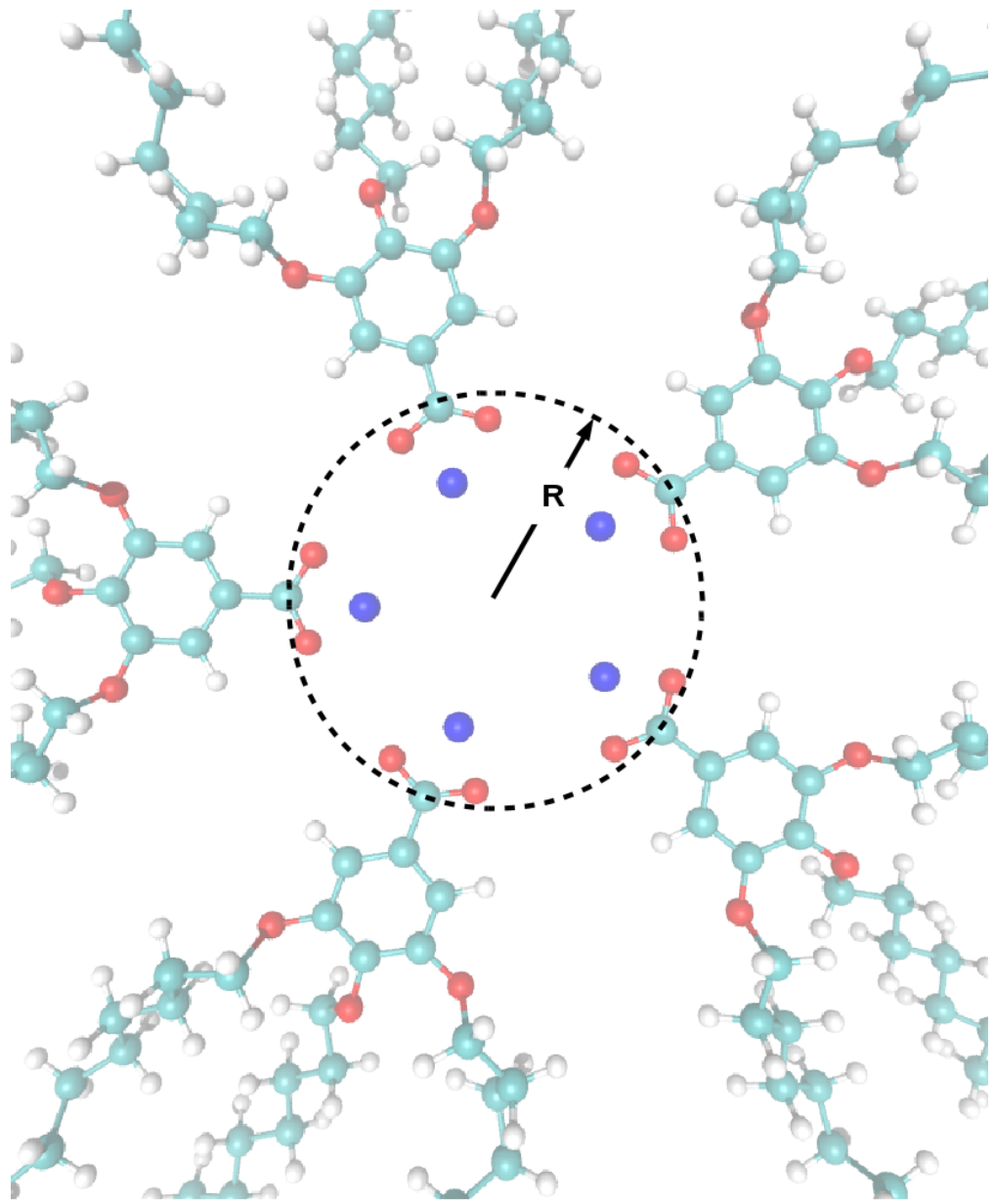


Figure 4: When creating an initial configuration, the pore radius is defined based on the distance of the carbonyl carbon from the pore's central axis

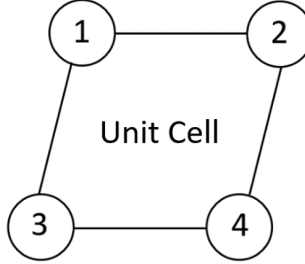


Figure 5: There are five pore-to-pore distances that are equal in a perfect hexagon. If each number in the diagram represents the center of a pore in a hexagonal unit cell, then the distance from 1 to 2, 2 to 4, 4 to 3, 3 to 1 and 1 to 4 should be equal. Only 4 of the distances are independent. For example, the distance from 1 to 4 is defined by the location of all other pore centers.

2. We calculated how long it takes for the data in each of the 5 trajectories to become uncorrelated using `pymbar.timeseries.integratedAutocorrelationTime()` [8, 9].
3. We broke the full equilibrated trajectory into blocks of length τ , where τ is the maximum of the five autocorrelation times calculated. Each block contains five sub-trajectories of pore-to-pore spacings.
4. We generate statistics using the bootstrapping technique. For each bootstrap trial, we reconstruct an equilibrium trajectory by randomly sampling from the trajectory blocks.
5. The average pore-to-pore distance is the mean of all pore spacings among all bootstrap trials.
6. To calculate the uncertainty in pore-to-pore distance, we calculate the average pore spacing for each pore over all bootstrap trials. Using the 5 average pore-to-pore distances, we calculate the spread with:

$$s = \sqrt{\frac{1}{4} \sum_{i=1}^5 (x_i - \bar{x})^2} \quad (1)$$

where \bar{x} is the average pore-to-pore distance.

Experimental correlation length of R- π

Experimentalists did not measure the correlation length, so we estimated it from the raw data. We took a slice of the 2D WAXS data along the dashed line in Figure 6a. We removed background noise by subtracting the intensity far from the pattern (high q) uniformly. We used a least squares algorithm to fit a lorentzian curve to the data. Only values recorded above $q_z = 1.6$ were considered for the fit in order to mitigate interference from R-alkanes (Figure 6b). The full width at half maximum (FWHM) is related to the correlation length, L , by the relationship: $L = \frac{1}{FWHM}$. The error in the value is calculated as the square root of the diagonal entry of the covariance matrix of optimized fit parameters.

Initial Configuration Dependence

We addressed any major dependence on initial configuration in the main text. There we showed that systems are stable when made with 4, 5, 6, 7, and 8 monomers per layer. We also showed that systems are stable when monomer head groups are oriented in the parallel displaced and sandwiched configurations (See Figure 3). Our model is most consistent with experiment when built with 5 monomers per layer, with layers stacked 3.7 Å apart in the parallel displaced configuration.

There are three other parameters whose choice may influence the equilibrium structure: initial pore spacing, initial pore radius and initial distance between layers. Here we show the results of a sensitivity analysis performed on the three parameters. To reduce the size of the sensitivity analysis, we only tested systems built with 5 monomers per layer with layers stacked in the parallel displaced configuration. We equilibrated all systems according to the dry equilibration procedure.

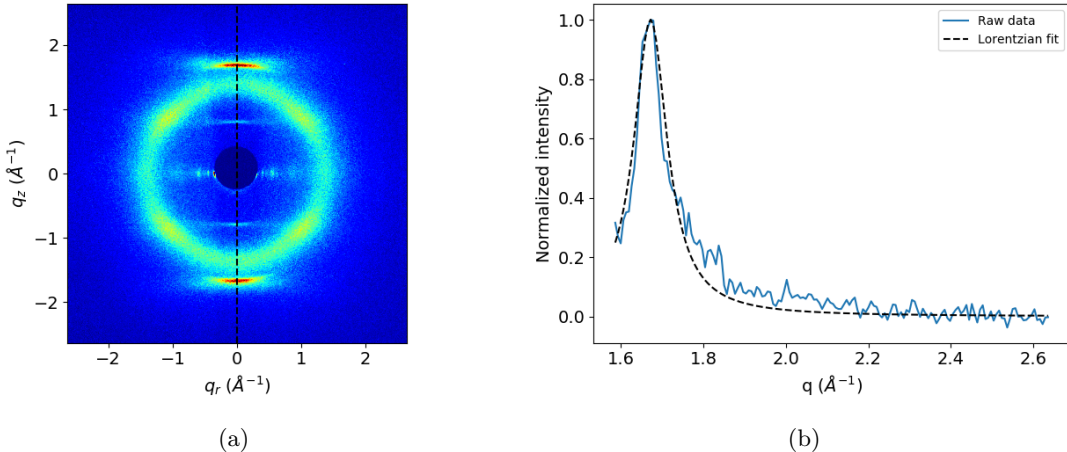


Figure 6

1. Initial pore spacing

We tested five different initial pore spacings, defined as the distance between the central axis of each pore with all others (Figure 7). To reduce the number of variables, we held the pore radius constant, at 6 Å and the distance between layers at 3.7 Å since those were the values used in our optimal system in the main text. We prioritized ensuring that resulting configurations maintain the expected hexagonal symmetry. If initial pore spacing is too small, we observe repulsion between columns which disrupts equilibration. If the pore spacing is too large the pores squeeze together, but in a distorted hexagonal array because the xy initial translation of the pores is somewhat erratic.

- (a) 39 Å : We tested a pore spacing of 39 Å in order to have a test system with an intial spacing below the experimental value. As soon as the restraining potential switches to 56 KJ mol⁻¹ nm⁻², the columns are able to repel resulting in a large jump in pore spacing (Figure 8a). After 400 ns, the pore spacing is 4.05 ± 0.17 nm. There is a large uncertainty in this value because the 1-4 pore spacing (Figure 7) deviates significantly from all other pore spacings. The 1-4 pore spacing is 4.31 nm while the average of all other pore spacings is 3.96 nm. The system deviates from hexagonal geometry and is trending towards cubic packing.
- (b) 41 Å : We chose to test a pore spacing of 41 Å since it closely matches the experimental pore spacing. Again, we observe abrupt repulsion of columns once the restraining potential is switched to 56 KJ mol⁻¹ nm⁻² (Figure 8b). After 400 ns, the average pore spacing settles below the experimental value at 4.07 ± 0.21 nm. Again, a large uncertainty in this value occurs because the 1-4 pore spacing (Figure 7) deviates significantly from all other pore spacings. The 1-4 pore spacing is 4.44 nm while the average of all other pore spacings is 3.96 nm.
- (c) 45 Å : A pore spacing of 45 Å is about 10 % larger than the experimental value. We observe relatively stable pore spacing during the restrained portion of the dry equilibration procedure (Figure 8c). The equilibrated pore spacing is 4.23 ± 0.03 nm. The system maintains hexagonal symmetry and exhibits the lowest uncertainty in pore spacing. We chose to use this value for all our simulations in the main text.
- (d) 50 Å : We tested a pore spacing of 50 Å, about 20 % larger than the experimental value. Once the restraining potential reaches 56 KJ mol⁻¹ nm⁻², the pore spacing begins to decrease linearly (Figure 8d). After 400 ns, the average pore spacing is 4.37 ± 0.13 nm. There is a large uncertainty with this value because, again, the array of pores deviates from hexagonal character. Using Figure 7 as a reference, pore 2 drifts outward from the array and forces the 1-4 distance to shrink in response.

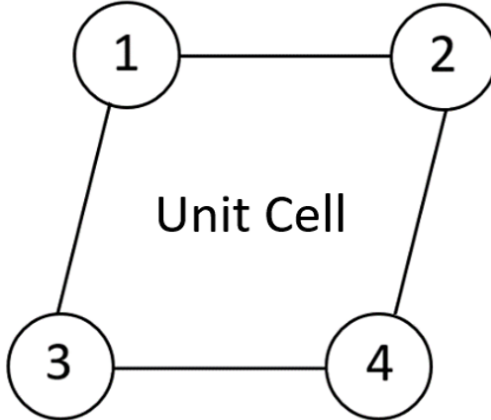


Figure 7: In a perfect hexagonal, there are 5 distances that should be exactly equal. As pictured in this diagram the distance from 1-2, 1-3, 1-4, 2-4, and 3-4 are the same.

- (e) 55 Å : We tested a pore spacing of 55 Å which is at a distance where monomers in each pore no longer intersect adjacent pores. Once the restraining potential reaches 56 KJ mol⁻¹ nm⁻², the pore spacing changes erratically until it begins to settle when the force constants are below 3 KJ mol⁻¹ nm⁻² (Figure 8e). We recommend avoiding a system such as this where vacuum gaps between pore columns are introduced unnecessarily. The system equilibrates to a pore spacing of 4.27 ± 0.18 nm. The 1-2 pore spacing is the outlier in this case with a pore spacing of 3.99 Å which distorts the hexagonal array.

2. Initial pore radius

We tested 3 different pore radii, defined as shown in Figure 4. For each system, we held the initial pore spacing constant at 45 Å and the initial distance between layers constant at 3.7 Å. Equilibrated values of pore radii are presented in Table 1. The pore radius in each simulation frame is calculated as the average distance of all carbonyl carbons (See Figure 4) from their associated pore center. Statistics for the pore radii reported were generated from the timeseries representing the average pore radius at each frame. We detected equilibration using `pymbar.timeseries.detectEquilibration`. We calculated the average and standard deviation of pore radii using only data points collected after equilibration was detected.

- (a) 2.5 Å : The smallest pore radius that we can achieve before energy minimization becomes problematic is 2.5 Å. After being run through the full dry equilibration procedure, the average pore radius is 0.40 ± 0.01 Å.
- (b) 5 Å : We tested a pore radius of 5 Å because it is slightly larger than the equilibrated pore radius of the system simulated with an initial pore radius of 2.5 Å. After being run through the full dry equilibration procedure, the average pore radius is 0.42 ± 0.01 Å, which agrees with the 2.5 Å configuration within error.
- (c) 8 Å : The largest pore radius that can be achieved before energy minimization becomes problematic is 8 Å. One should use caution with such a structure because of the relatively large vacuum space that is created in the pore region of the initial configuration. After being run through the full dry equilibration procedure, we see a combination of cylindrical and slit-like pores (Figure 9). Measuring the pore radius of this system does not have a concrete meaning since slits do not have a single radius, but its calculated value is reported in Table 1. We are wary of such a non-symmetric structure and choose not to use a pore radius of 8 Å for our starting configurations.

3. Initial distance between layers

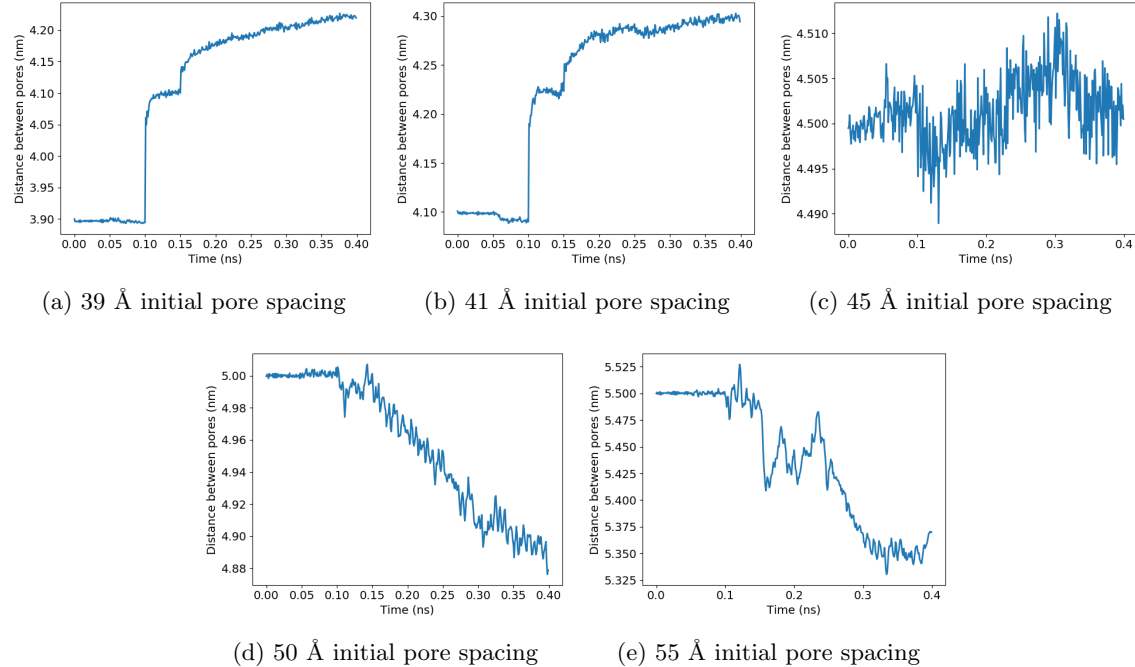


Figure 8: The pore spacing during the restrained portion of the dry equilibration procedure is shown. Every 50 ps (0.05 ns) position restraints are reduced according to the sequence: 1000000, 3162, 56, 8, 3, 2, 1, 0 KJ mol⁻¹ nm⁻². When the initial pore spacing is chosen below the experimental value (a) or at the experimental value (b), there is an abrupt change in pore spacing when the position restraints are reduced to 56 KJ mol⁻¹ nm⁻². When pores are started 45 Å apart (c) the pore spacing remains relatively stable. When pores are spaced 50 Å apart (d), the pore spacing decreases nearly linearly once the restraints are reduced to 56 KJ mol⁻¹ nm⁻². When pores are spaced 55 Å apart (e), so that monomers do not intersect with adjacent pores, and position restraints are reduced to 56 KJ mol⁻¹ nm⁻², the pore spacing changes erratically before stabilizing when force constants are reduced below 3 KJ mol⁻¹ nm⁻².

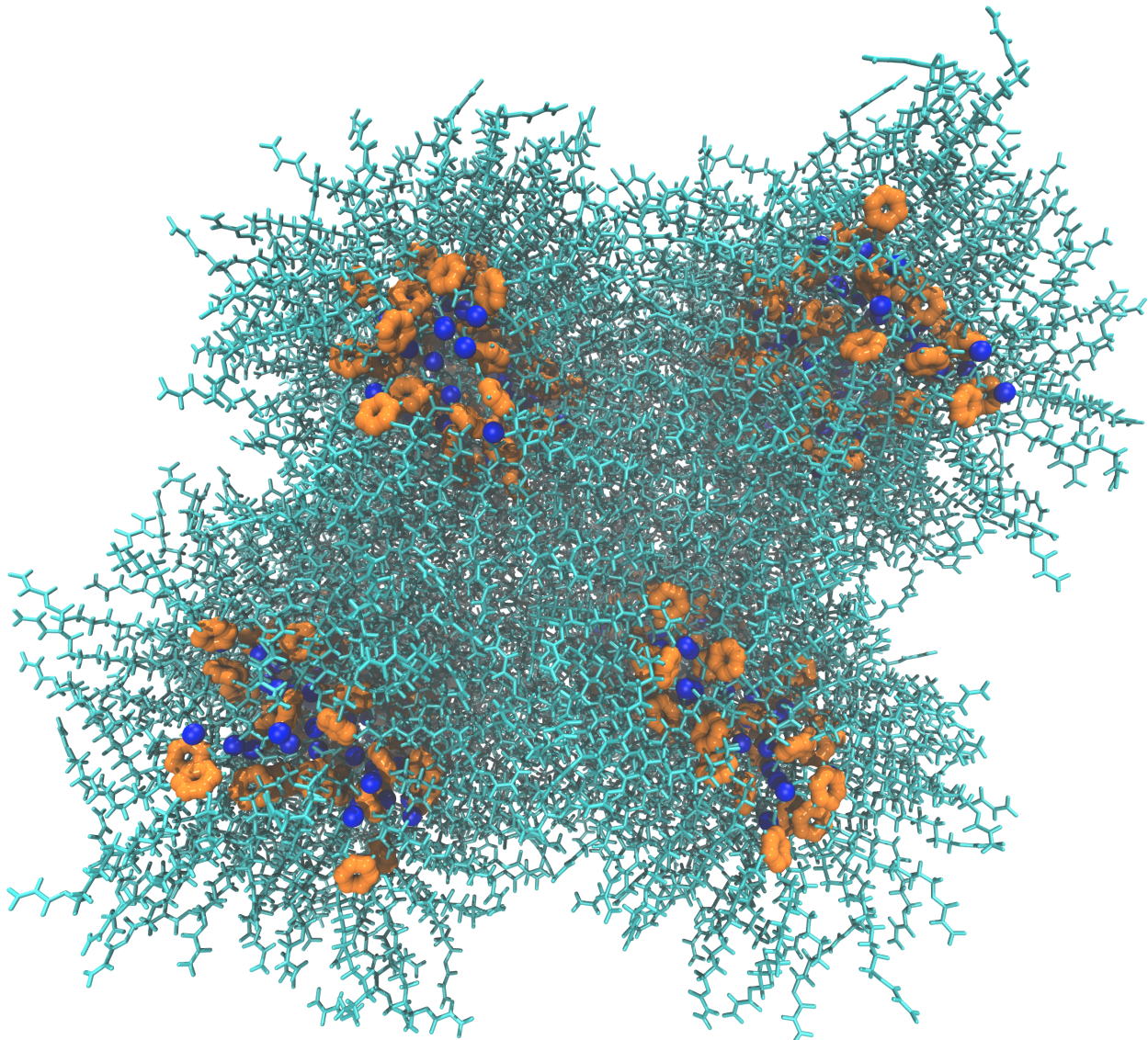


Figure 9: A system that was built with an initial pore radius of 8 Å equilibrates to a structure that exhibits both cylindrical and slit-like pores. As pictured here, sodium ions are colored blue, carbon atoms in the aromatic ring of the head group are colored orange and all else is colored cyan.

Initial Pore Radius	Equilibrated Pore Radius
2.5 Å	0.40 ± 0.01 Å
5 Å	0.42 ± 0.01 Å
8 Å	0.69 ± 0.01 Å

Table 1: The average pore radii of systems built with an initial pore radius of 2.5 Å and 5 Å equilibrate to values that agree within error. If the pore radius is too large, slit pores may form.

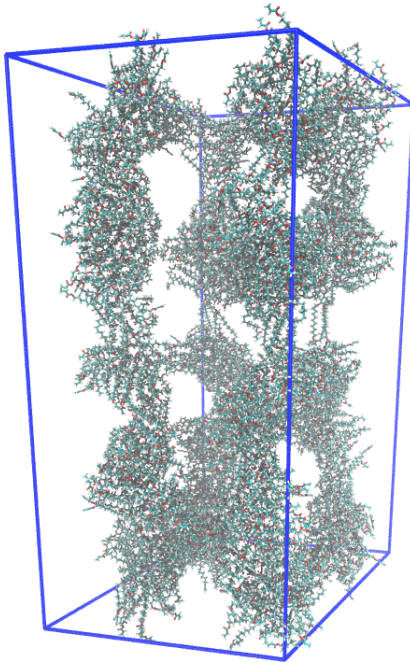


Figure 10: When layers are initially stacked 10 Å apart and the system is equilibrated using the dry equilibration procedure, large vacuum gaps form as the monomers attempt to fill space.

We tested 3 different initial layer spacings, defined as the distance between the planes of aromatic rings in each layer. Systems built with layers stacked 3.7 Å and 5 Å apart are discussed extensively in the main text. We will focus the discussion here on systems built with layers stacked 10 Å apart.

Figure 10 shows the structure of an assembly built with an initial layer spacing of 10 Å immediately after the restrained portion of the equilibration procedure. Since we used position restraints, the simulations were run in the NVT ensemble. When layer spacing is large, such as this situation, there is a significant amount of vacuum space which the monomer attempts to fill. Even if turning pressure control on allows the system to recover the geometry of the hexagonal phase, we would likely need much longer equilibration times, and it will almost certainly get trapped in a metastable configuration that bears no resemblance to the experimental profile.

Crosslinking Mechanism

Crosslinking of the monomer Na-GA3C11 occurs by a UV initiated free radical polymerization (Figure 18). Head-to-tail addition takes place between terminal vinyl groups on each of the monomer tails. We only considered head-to-tail addition since it is the dominant propagation mode in the real system.

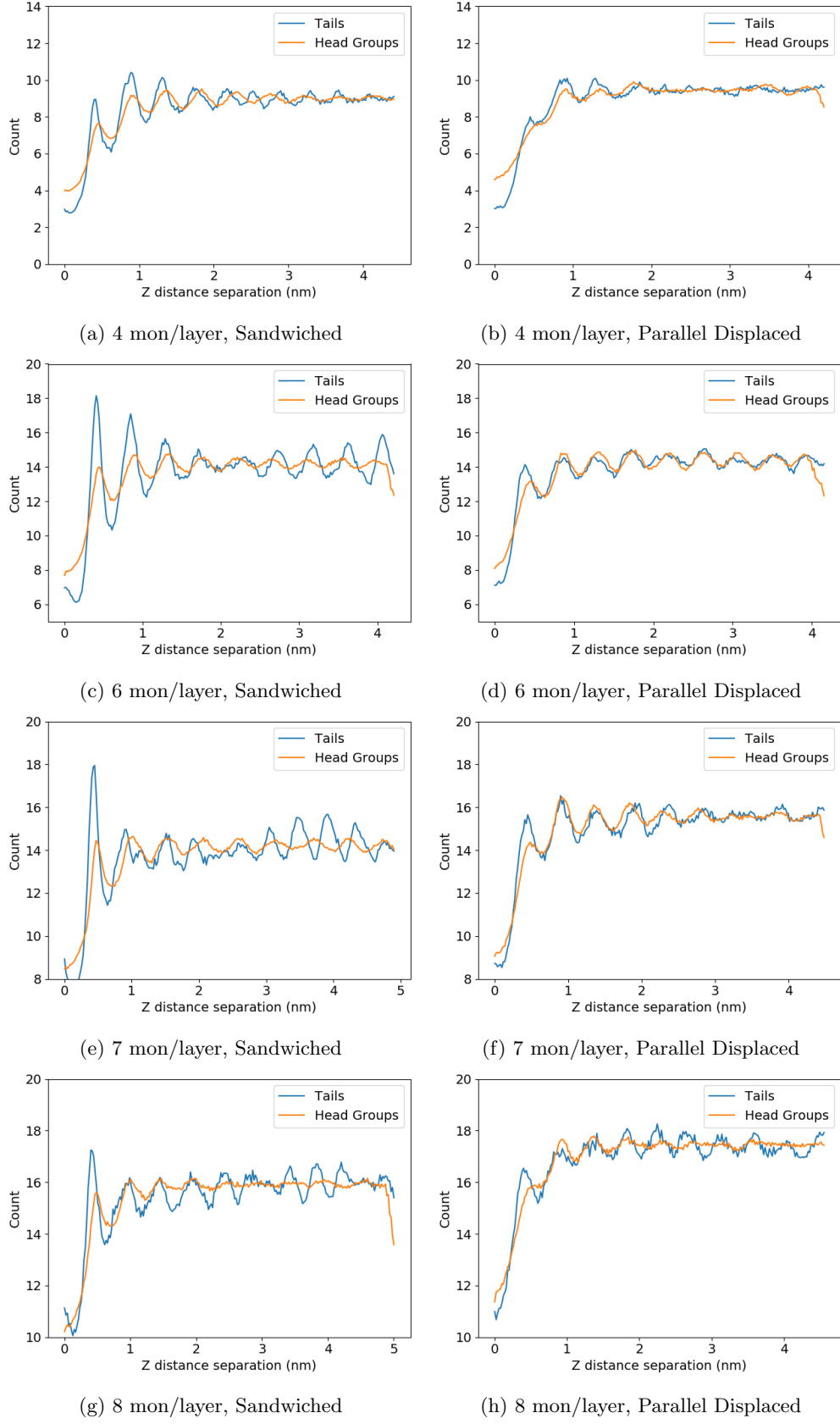


Figure 11: $g(z)$ for all other configurations built with layers stacked 3.7 Å apart

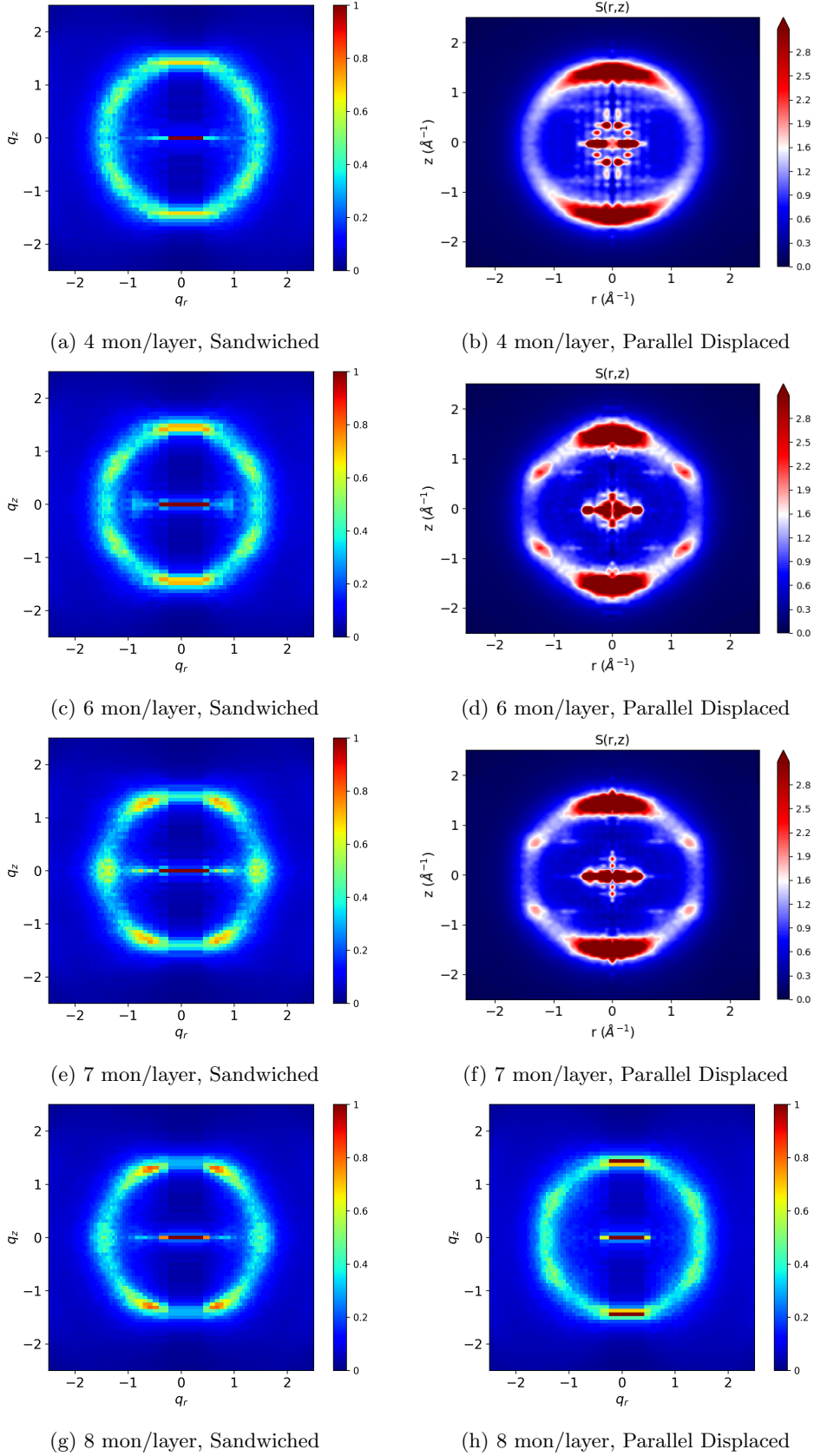


Figure 12: Simulated XRD patterns for all other configurations built with layers stacked 3.7 Å apart

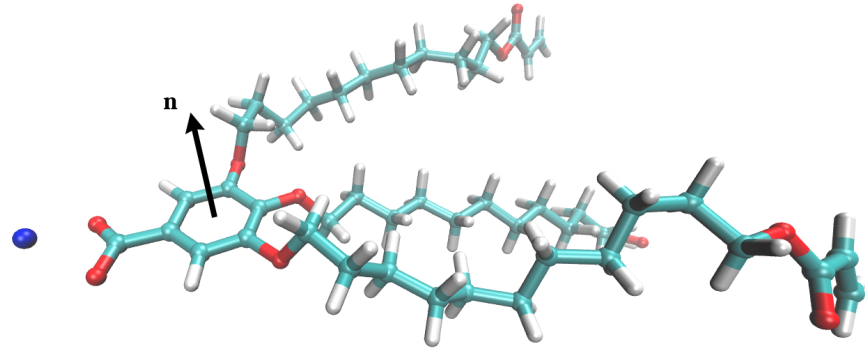


Figure 13: We define the nematic director vector, \mathbf{n} , as the vector perpendicular to the plane of the aromatic head group.

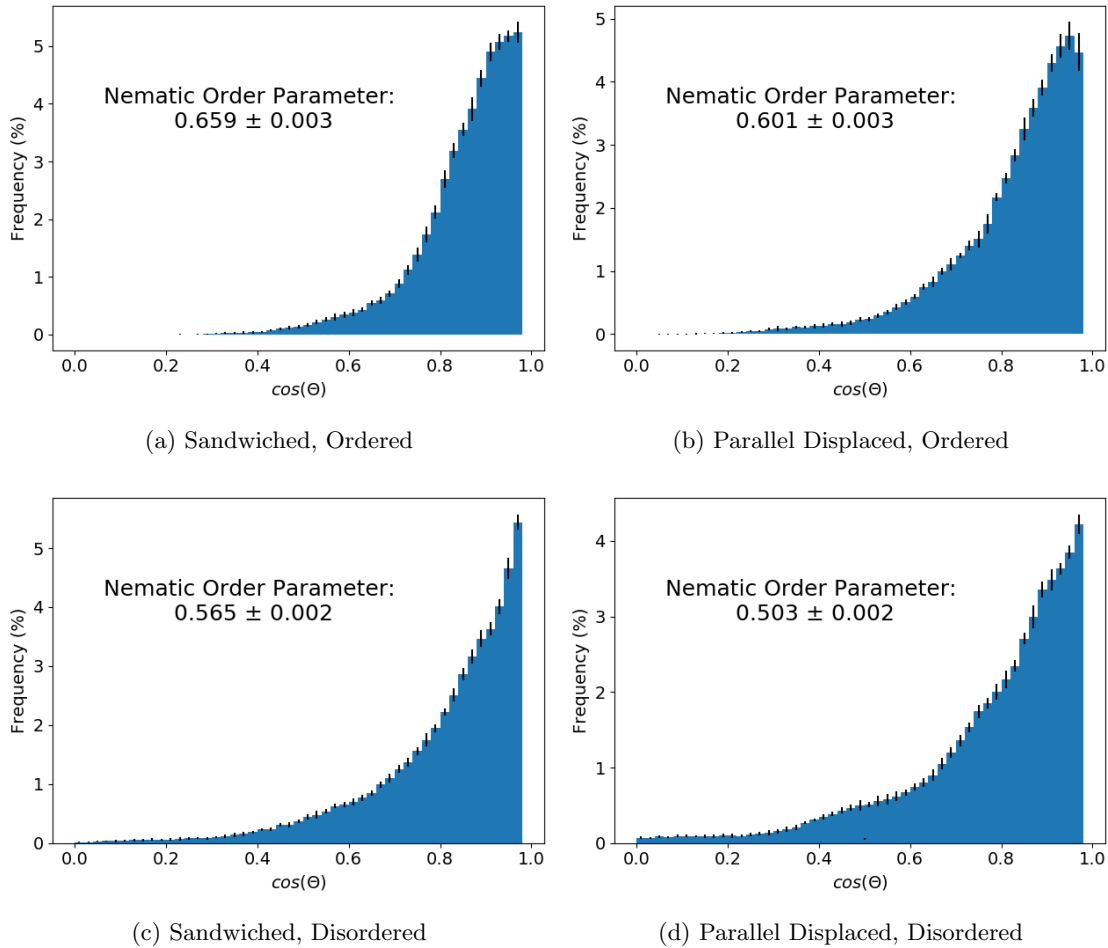


Figure 14: The distribution of angles between nematic director vector (See Figure 13) and the z-axis averaged over the equilibrated portion of each trajectory

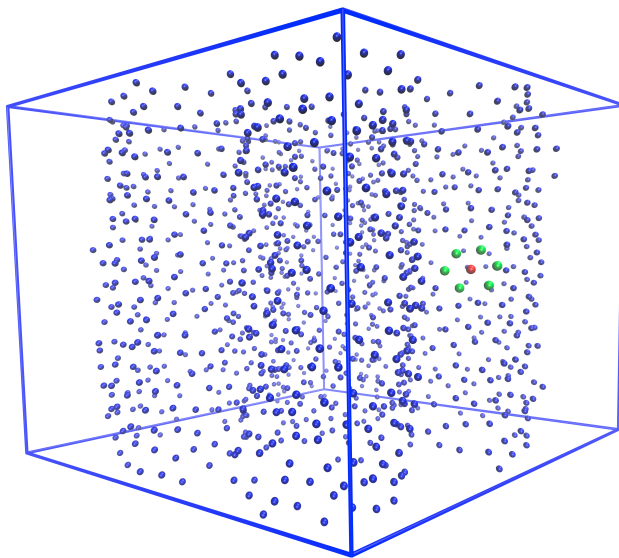


Figure 15: Monomer tails pack together hexagonally. The centroid of each tail is visualized as a blue sphere. The centroids are calculated based on the red atoms in Figure 2. The red sphere highlights an example of an alkane tail centroid with its nearest neighbors (green spheres) surrounding it in a hexagonal pattern.

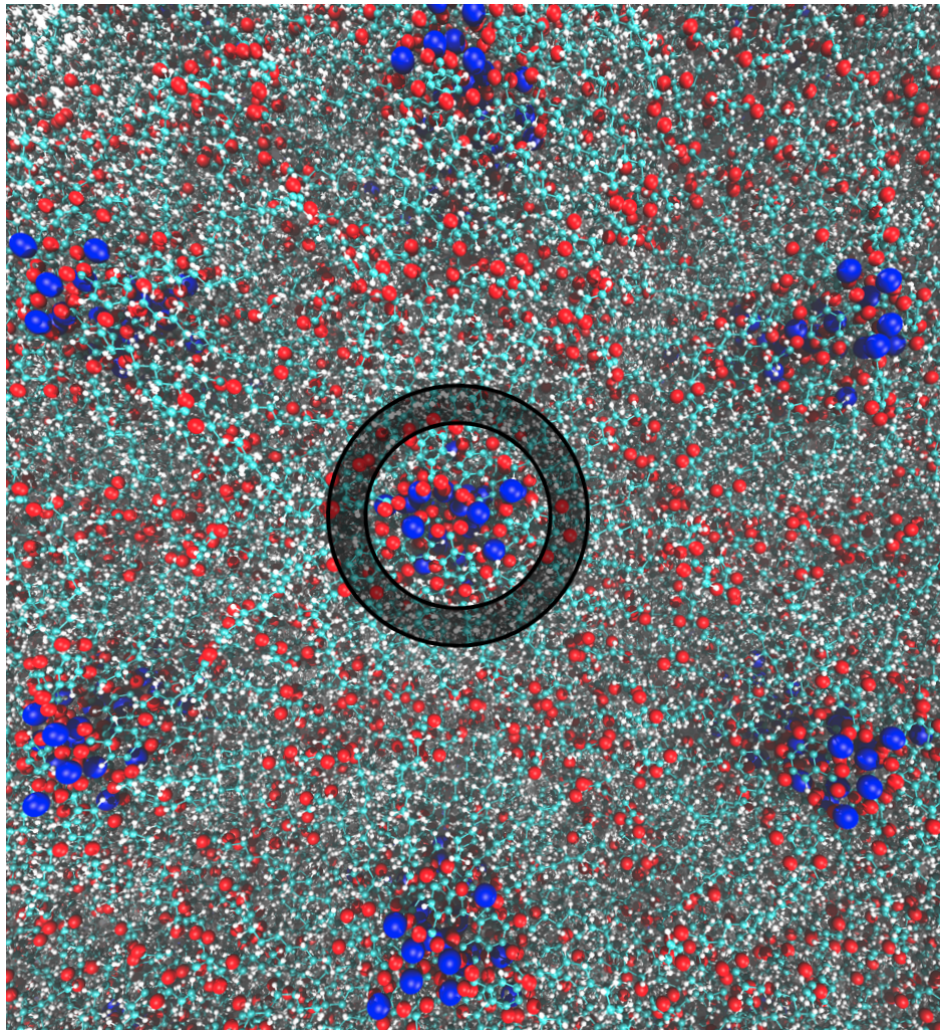
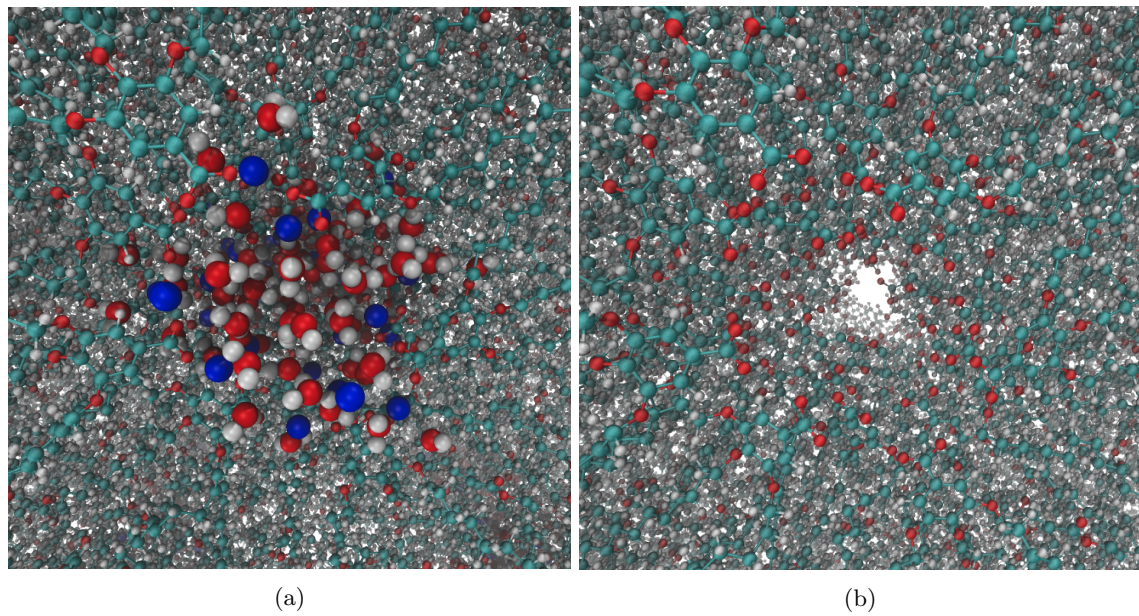


Figure 16: Looking down onto the plane of membrane, this diagram illustrates how we calculated radial distribution functions. We binned the radial distance of all atoms in chosen groups from pore centers. The pore centers are defined as the average coordinates of sodium ions in each pore. The bins are defined by the annulus bounded by concentric circles centered at the pore centers, as shown. To normalize, we divide the count of atoms within the bin annulus by the volume of the annulus where the volume is the area of the annulus times the height of the membrane in the z-direction.



(a)

(b)

Figure 17: (a) Pores built in the parallel displaced configuration with 5 monomers per layer are filled with 5 wt% water. (b) The same system is visualized with water molecules and sodium ions removed. Head groups vacate the pore region leaving an aqueous solution of water and sodium ions.

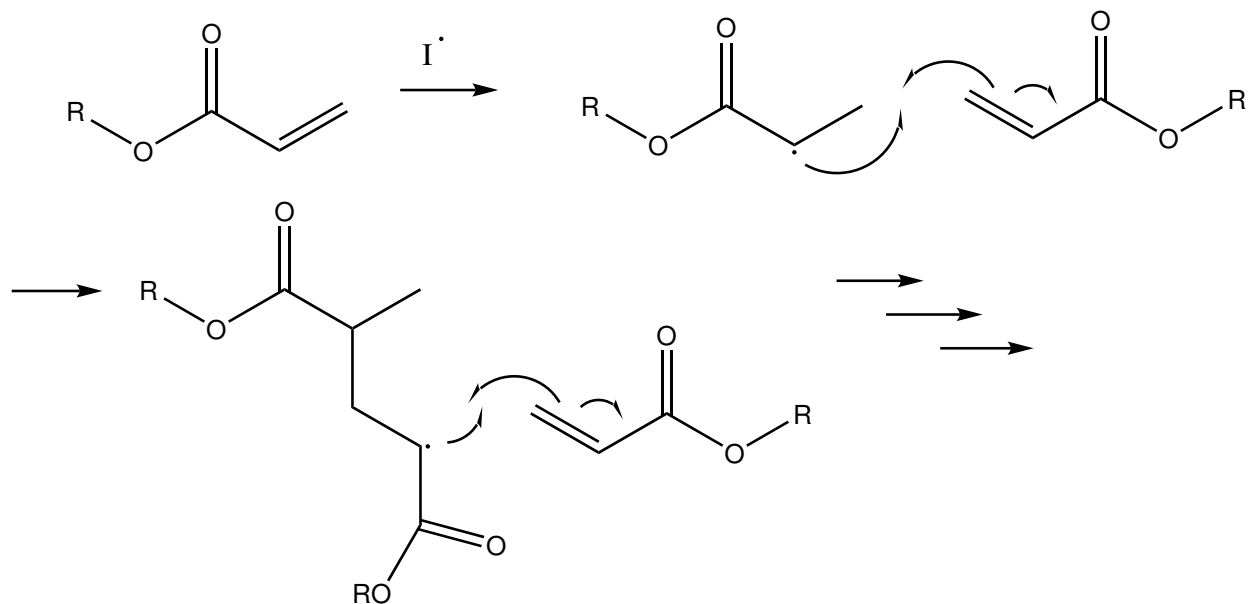


Figure 18: Terminal vinyl groups present on each monomer tail react with free radical initiators to create monomers with terminal vinyl radicals. Vinyl radicals react with the vinyl groups of other monomers in to propagate crosslinking.

References

- [1] ChemAxon, “MarvinSketch 17.13 2017 ChemAxon (<http://chemaxon.com>),” 2017.
- [2] N. M. O’Boyle, M. Banck, C. A. James, C. Morley, T. Vandermeersch, and G. R. Hutchison, “Open Babel: An open chemical toolbox,” *Journal of Cheminformatics*, vol. 3, p. 33, Oct. 2011.
- [3] “The Open Babel Package, version 2.4.1 <http://openbabel.org>.”
- [4] J. Wang, W. Wang, P. A. Kollman, and D. A. Case, “Automatic atom type and bond type perception in molecular mechanical calculations,” *Journal of Molecular Graphics and Modelling*, vol. 25, pp. 247–260, Oct. 2006.
- [5] D. Case, R. Betz, W. Botello-Smith, D. Cerutti, T. Cheatham, III, T. Darden, R. Duke, T. Giese, H. Gohlke, A. Goetz, N. Homeyer, S. Izadi, P. Janowski, J. Kaus, A. Kovalenko, T. Lee, S. LeGrand, P. Li, C. Lin, T. Luchko, R. Luo, B. Madej, D. Mermelstein, K. Merz, G. Monard, H. Nguyen, H. Nguyen, I. Omelyan, A. Onufriev, D. Roe, A. Roitberg, C. Sagui, C. Simmerling, J. Swails, R. Walker, J. Wang, R. Wolf, X. Wu, L. Xiao, D. York, and P. Kollman, “AmberTools16,” Apr. 2016.
- [6] R. Walker and S. Tang, “Antechamber Tutorial (ambermd.org/tutorials/basic/tutorial4b/)”
- [7] A. W. Sousa da Silva and W. F. Vranken, “ACPYPE - AnteChamber PYthon Parser interfacE,” *BMC Research Notes*, vol. 5, p. 367, July 2012.
- [8] J. D. Chodera, “A Simple Method for Automated Equilibration Detection in Molecular Simulations,” *Journal of Chemical Theory and Computation*, vol. 12, pp. 1799–1805, Jan. 2016.
- [9] M. R. Shirts and J. D. Chodera, “Statistically optimal analysis of samples from multiple equilibrium states,” *The Journal of Chemical Physics*, vol. 129, p. 124105, Sept. 2008.